Monte Carlo Simulation of Models for Single Polyethylene Coils

J. Baschnagel,* K. Qin,† W. Paul, and K. Binder

Institut für Physik, Johannes-Gutenberg-Universität Mainz, Staudinger Weg 7, D-6500 Mainz, West Germany

Received June 24, 1991; Revised Manuscript Received February 3, 1992

ABSTRACT: A variant of a simple sampling Monte Carlo technique is applied to study the configurational statistics of models for short isolated polyethylene chains, taking into account variations of the bond lengths, the bond angles, and the torsional angles as well as a Lennard-Jones (LJ) potential between nonbonded neighbors. The dependence of the mean-square end-to-end distance $\langle R^2 \rangle$, of the gyration radius $\langle R_g^2 \rangle$, and of their ratio $\langle R^2 \rangle / \langle R_g^2 \rangle$ on temperature T and chain length N is studied. We also investigated the characteristic ratio $C_\infty(T)$ and distribution functions $P_n(l)$ and $P_n(\vartheta)$, where l stands for the length of groups formed from n successive monomers and ϑ for the angle between two such successive groups. In a Θ-solvent or a dense melt the LJ interaction will be screened due to the polarizability of the solvent or due to other chains, respectively. We model this with a cutoff in the LJ interaction and show that all data depend very sensitively on the way in which the Lennard-Jones potential is truncated. Furthermore, we note that different potential models for polyethylene yield significantly different results. In view of these problems, it is not obvious that one can identify such configurations of isolated single chains with coil configurations in either Θ-solvent or a dense melt, respectively. Possible consequences for various approaches toward the chemically realistic modeling of polymeric materials are briefly discussed.

1. Introduction

Recently there has been much interest in applying atomistic simulation (such as molecular dynamics[1-4] (MD) or Monte Carlo[5-10] (MC) techniques) to chemically realistic models of macromolecular chains.[11-18] The correlation between the macroscopic physical properties of these materials and their chemical structure is a challenging goal of these studies and of related work.[19,20]

However, the application of such atomistic simulation methods to macromolecular systems is not at all straightforward, due to the enormous spread in both length scales and time scales:[10,21,22] a single coil with $N \approx 500$ monomers exhibits structure from the bond length (~1 Å) to the persistence length[23] (~10 Å) to the coil radius R (~10^2 Å); in an entangled melt, the time scales range from the bond angle vibration time τ_{vib} (~10^{-13} s) to slow processes on local scales (e.g., bond reorientational jumps in the torsional potential, with a relaxation time $\tau_1 \sim 10^{-11}$ s, for instance) and to very slow motions on large scales. For instance, assuming a typical entanglement degree of polymerization $N_e \approx 50$, reptation theory[24] implies a relaxation time for the chain configuration as $\tau_N \approx \tau_1 \cdot (N/N_e)N^2 \approx 10^{-5}$ s, i.e., exceeding τ_{vib} by 8 orders of magnitude. Since in MD the elementary time step Δt should be much smaller than the shortest physical time scale (τ_{vib}), an atomistically detailed MD simulation of well-equilibrated entangled melts seems to be very difficult. The MD simulation of Kremer and Grest,[4] who studied entangled melts of simple bead spring chains, already needed over 1000 Cray XMP hours. Even if one restricts the application of this technique to melts of much shorter nonentangled chains[13-16] or to single chains,[18] it is a computationally demanding and nontrivial task to reach proper equilibration employing a MD technique.

Being interested in the configurational statistics or other static properties of single polymer chains, MC techniques with their enormous flexibility in the choice of the elementary move will be superior to MD techniques in the generation of statistically independent configurations. For the MC simulation one would not follow the original Metropolis procedure,[25] appropriate for simple monatomic fluids, where atoms are randomly moved from an old position $\vec{r}$ to a new position $\vec{r}' = \vec{r} + \Delta\vec{r}$ and where the displacement vector $\Delta\vec{r} = (\Delta x, \Delta y, \Delta z)$ is chosen completely at random (and hence blindly) from some interval $-\delta \leq \Delta x, \Delta y, \Delta z < +\delta$. Such an arbitrary choice of the displacement vector $\Delta\vec{r}$ will generally not correspond to values of the bond length, the bond angle, and the torsional angle, which are energetically favored by the microscopic chain potentials. Therefore, the Metropolis transition probability and, as a corollary, the acceptance rate for such moves would typically be very small, unless δ is chosen extremely small, which then inevitably means the convergence of the algorithm is drastically slowed down. But the advantage of MC is that the MC steps can be adjusted to the particular potentials at hand, and in this way an efficient sampling of the full configurational space is straightforwardly possible.

This idea is exemplified in the present work, where the configurational properties of single polyethylene (PE) chains are investigated, using a model potential that has been used for recent MD work[15] but applying a kind of generalized simple sampling MC technique instead. Attention is focused on the question of to what extent properties of such chains can be identified with properties of chains in either Θ-solution or a dense melt, if one suitably cuts off the nonbonded interactions for distant neighbors along the chain. As is well-known, if one did not cut off this interaction, it would either lead to a swelling of the coil (if it is predominantly repulsive) or to a collapse (if it is predominantly attractive) corresponding to the behavior of single chains in either good or bad solvents,[26] which is outside of interest here. However, it will be demonstrated that it is very delicate to cut off this interaction properly, because most quantities do sensitively depend on the details of this procedure. Attention will also be paid to the question of to what extent different choices of model potentials for PE actually yield similar results.

The outline of this paper is as follows: section 2 summarizes the model and the simulation technique. Section 3 describes our results for the mean-square end-to-end distance $\langle R^2 \rangle$ of the chains and gyration radius

† Present and permanent address: Department of Physics, University of Peking, Peking, People's Republic of China.

0024-9297/92/2225-3117$03.00/0

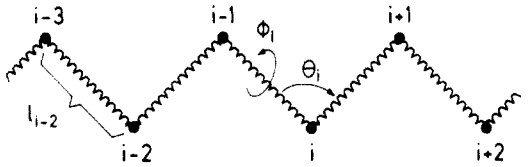

Figure 1. Schematic model of the PE chain. The spherical segment (labeled by index $i = 0, ..., N$) denotes a CH_2 unit. The segments are connected by harmonic bonds, the bond length being l_i. Three successive segments define a bond angle θ_i and four successive segments a torsional angle ϕ_i (which is zero in the planar all-trans configuration shown). It is the angle between the bonds formed from the segments $(i-2, i-1, i)$ and $(i-1, i, i+1)$. Segments separated by more than three bonds along the chain (e.g., segments $i-3$ and $i+1$) interact according to a truncated Lennard-Jones potential.

$\langle R_g^2 \rangle$, for the case where the nonbonded interactions are completely cut off and the simulation algorithm can be checked by a simple extension of Flory's transfer matrix methods.[23] Section 4 contains simulation results including the nonbonded interaction and studies the effect of varying the cutoff. While these sections focus on the global configurations of the chains, section 5 discusses their local structure in terms of the distributions $P_n(l)$ for the length l of groups formed from n successive monomers, choosing $n = 5$ and 10 as an example, as well as the distribution $P_n(\vartheta)$ of the angle ϑ between two successive groups. Section 6 summarizes our conclusions and gives an outlook for further works.

2. The Model and the Simple Sampling Technique

Even for polyethylene, a chemically simple polymer, there is not yet an agreement which is the "best" model potential.[11-16,22,27-29] In this work we use a model which was taken in previous MD work[15-17] which includes bond length and bond angle vibrations along the backbone of the PE chain (Figure 1) but treats the CH_2 monomers as "united atoms". For a chain of $N+1$ monomers, which are labeled by an index $j = 0, 1, 2, ..., N$, the Hamiltonian is

$$\mathcal{H} = \sum_{j=1}^{N} \mathcal{H}_l(l_j) + \sum_{j=1}^{N-1} \mathcal{H}_\theta(\theta_j) + \sum_{j=2}^{N-1} \mathcal{H}_\phi(\phi_j) + \sum_{i \neq j}{}' \mathcal{H}_{LJ} \qquad (1)$$

where the first term represents bond length vibrations, the second bond angle vibrations, the third the torsional potential, and the last the nonbonded interaction. These contributions to the Hamiltonian are taken to be

$$\mathcal{H}_l(l_j) = \frac{f_l}{2}(l_j - l_0)^2 \qquad (2)$$

$$\mathcal{H}_\theta(\theta_j) = \frac{f_\theta}{2}(\cos\theta_j - \cos\theta_0)^2 \qquad (3)$$

$$\mathcal{H}_\phi(\phi_j) = f_\phi \sum_{n=0}^{5} a_n \cos^n \phi_j \quad (a_0 \equiv 1) \qquad (4)$$

and the nonbonded interactions are taken to be of the Lennard-Jones (LJ) form

$$\mathcal{H}_{LJ} = 4\epsilon\{(\sigma/r_{ij})^{12} - (\sigma/r_{ij})^6\} \qquad (5)$$

Here l_j denotes the length of the bond connecting monomers $j-1$ and j (Figure 1), θ_j denotes the bond angle, and the ϕ_j denotes the torsional angle. The constants f_l, l_0, f_θ, $\cos\theta_0$, f_ϕ, a_0, a_1, a_2, a_3, a_4, a_5, ϵ, and σ are collected in Table I. The Euclidean distance between segments i and j is denoted by r_{ij}. Note that the prime in the last sum in eq 1 means that this term is included only for monomers which are at least four units apart along the backbone of the chain. In addition, the potential in eq 5 is truncated at $r_{ij} = 1.5\sigma$. This truncation distance may seem unusually short, but we choose it to be the same as in refs 15 and 16, because we wanted to work with exactly the same model.

Table I
Parameters for the Rigby-Roe Model of Polyethylene[15]

l_0, nm	0.152	a_3	−0.3297
$\cos\theta_0$	−0.3333	a_4	2.828
f_b, J nm^2 mol^{-1}	3.46×10^7	a_5	−3.3943
f_θ, J mol^{-1}	5×10^5	$\Delta E(t \rightarrow g^\pm)$, J mol^{-1}	2842
f_ϕ, J mol^{-1}	9×10^3	ΔU_1, J mol^{-1}	11978
a_0	1	ΔU_2, J mol^{-1}	43444
a_1	1.31	ϵ, J mol^{-1}	500
a_2	−1.414	σ, nm	0.38

The potential specified above means a cutoff of the nonbonded interaction in space. This can only lead to the two following cases: Depending on the cutoff distance and on the temperature, the effective interaction will be either predominantly repulsive, resulting in a "swollen" coil relating to a good solvent ($\langle R^2 \rangle \sim N^{2\nu}$ with $\nu \simeq 0.59$),[26] or predominantly attractive, resulting in a "collapsed" coil relating to a bad solvent ($\langle R^2 \rangle \sim N^{2/3}$). Only for a particular temperature (the Θ temperature), which depends on the potential parameters and the cutoff distance, will the coil exhibit Gaussian behavior ($\langle R^2 \rangle \sim N$). A cutoff in space therefore will at general temperatures not lead to Gaussian chains corresponding to Θ conditions or to polymer melts,[23,26] if one does not explicitly treat a many-chain system. To mimic the effect of the interactions with the solvent particles or the other chains in the bulk, in a simulation of a single chain one has to employ a cutoff of the nonbonded interaction *along the chain*. Thus we have put $\mathcal{H}_{LJ} \equiv 0$, if the distance $|i-j|$ along the chain is larger than a certain cutoff Δ_{max}, because then eq 5 is a short-range interaction along the chain and the configuration of the chain, for large N, *must* be a Gaussian coil, irrespective of the magnitude of Δ_{max}. The variation of Δ_{max} can be viewed as a variation of the blob size.[26] Inside the blob the excluded-volume interaction leads to a local swelling of the chain, whereas the whole chain itself will be a random walk of blobs obeying Gaussian statistics. However, some quantitative characteristics of the coil such as the ratio C_∞ (defined from the relation $\langle R^2 \rangle \rightarrow C_\infty \langle l^2 \rangle N$ as $N \rightarrow \infty$) will depend on this cutoff, and hence we have investigated the effect of diferent choices for Δ_{max}, namely, $\Delta_{max} = 3$–5, 7, and 10 (note that $\Delta_{max} = 3$ means the LJ interaction is omitted altogether, and for $\Delta_{max} = 4$ a single distance along the chain has a nonzero LJ interaction).

We now describe the Monte Carlo technique used for sampling the chain configurations. Chains with length $N \leq 50$ have been generated. For this range of chain lengths, the easiest and also rather efficient approach is a variant of a simple sampling technique.[7,8] Let us first consider the case $\Delta_{max} = 3$, where the LJ interaction in eq 5 is neglected. Now it is straightforward to construct chain configurations directly proportional to the correct Boltzmann weight. [Z = partition function; for simplicity, we denote $\mathcal{H}_l(l_j) + \mathcal{H}_\theta(\theta_j) + \mathcal{H}_\phi(\phi_j)$ as $\mathcal{H}_j(l_j,\theta_j,\phi_j)$ with $\mathcal{H}_N(l_N,\theta_N,\phi_N) = \mathcal{H}_l(l_N)$ and define $\mathcal{H}_\phi(\phi_{j=1}) \equiv 0$. The symbol $\{l_j, \theta_j, \phi_j\}$ stands for the set of coordinates which

defines the chain's configuration.]

$$P[\{l_i,\theta_i,\phi_i\}] = \frac{1}{Z}\exp[-\mathcal{H}(\{l_i,\theta_i,\phi_i\})/k_BT] = \frac{1}{Z}\prod_{j=1}^{N}\exp[-\mathcal{H}_j(l_j,\theta_j,\phi_j)/k_BT] = \frac{1}{Z}\prod_{j=1}^{N}\{\exp[-\mathcal{H}_l(l_j)/k_BT]\exp[-\mathcal{H}_\theta(\theta_j)/k_BT]\times \exp[-\mathcal{H}_\phi(\phi_j)/k_BT]\} \quad (6)$$

since this probability simply factorizes into separate contributions for each degree of freedom. Thus we just build up the chain, taking one end as the origin of the coordinate system $\vec{r}_0 = 0$ and choosing the direction of the first bond ($j = 1$) along the x-axis of a space fixed coordinate system and the length of this bond according to the distribution $\exp[-\mathcal{H}_l(l_{j=1})/k_BT] = \exp[-(f_l/2k_BT)(l_{j=1} - l_0)^2]$. Thus the coordinate $\vec{r}_1$ of the second monomer, which is equal to the bond vector in this case, is straightforwardly determined.

For the bond vector of the next monomer $\vec{b}_2$ we have to choose $\cos\theta_{j=1}$ from a Gaussian distribution, $\exp[-(f_\theta/2k_BT)(\cos\theta_{j=1} - \cos\theta_0)^2]$, where $\phi_{j=1}$ is set to zero, as mentioned above, and the length $l_{j=2}$ is taken again from the appropriate Gaussian distribution. For the monomer $j = 3$ we have to use the torsional potential $\mathcal{H}_\phi(\phi_j)$ for the first time, since ϕ_j is to be chosen from its distribution $\exp[-\mathcal{H}_\phi(\phi_{j=2})/k_BT]$ in addition to the bond length and the bond angle. For this purpose the auxiliary distribution

$$P_\phi(\phi_i) = \frac{1}{Z_\phi}\int_{-\pi}^{\phi_i}\exp\left[-\frac{\mathcal{H}_\phi(\phi_i')}{k_BT}\right]d\phi_i' \quad (7)$$

where Z_ϕ is determined from the condition $\int_{-\pi}^{+\pi}P_\phi(\phi')\,d\phi' = 1$, is constructed. Then a random number ξ, uniformly distributed in the interval [0, 1], is drawn, and ϕ_i is obtained from requiring {($P_\phi(\phi_i)$ is calculated only once and stored in a table}

$$P_\phi(\phi_i) = \xi \quad (8)$$

Equation 8 then is solved for ϕ_i by a bisection method. This method is essentially equivalent to the one Milchev, Heermann, and Binder used in a finite-size scaling analyis of the ϕ^4-field theory[30] and Almarza et al. recently applied in a MC simulation of a liquid n-butane.[31] Note that also bond lengths l_i and angles $\cos\theta_i$ are constructed analogously, avoiding thus the (slower) routines yielding Gaussian random numbers.

The same procedure is then carried out for the rest of the monomers in the chain, which provides a representation of the chain's configuration in terms of the set $\{l_i, \theta_i, \phi_i\}$. For further analysis it is more convenient to know the coordinates of the monomers $\{\vec{r}_i\}$, which can be achieved as

$$\vec{r}_j = \vec{b}_1 + \mathbf{T}_1\vec{b}_2 + \mathbf{T}_1\mathbf{T}_2\vec{b}_3 + \ldots\mathbf{T}_1\ldots\mathbf{T}_{j-1}\vec{b}_j \quad (9)$$

$\mathbf{T}_i$ being the matrix that rotates the bond vector $\vec{b}_i$ into the direction of the bond vector $\vec{b}_{i-1}$.

$$\mathbf{T}_i = \begin{pmatrix} -\cos\theta_i & \sin\theta_i & 0 \\ \sin\theta_i\sin\phi_i & \cos\theta_i\sin\phi_i & \sin\phi_i \\ \sin\theta_i\sin\phi_i & \cos\theta_i\sin\phi_i & -\cos\phi_i \end{pmatrix} \quad (10)$$

For the simple problem where the LJ interaction (eq 5) is zero, one can apply the techniques of Flory[23] to calculate the mean-square end-to-end distance $\langle R^2\rangle$ and the gyration radius $\langle R_g^2\rangle$ exactly. The result for $\langle R^2\rangle$ is[28]

$$\langle R^2\rangle = N\langle l\rangle^2\left\{\frac{\langle l^2\rangle - \langle l\rangle^2}{\langle l\rangle^2} + C_\infty\right\} - \frac{2\langle l\rangle^2}{\lambda_2 - \lambda_1}\left[(\langle\cos\theta\rangle + \lambda_2)\frac{\lambda_1 - \lambda_1^{N+1}}{(1-\lambda_1)^2} - (\langle\cos\theta\rangle + \lambda_1)\frac{\lambda_2 - \lambda_2^{N+1}}{(1-\lambda_2)^2}\right] \quad (11)$$

with C_∞ being the characteristic ratio defined from $C_\infty = \lim_{N\to\infty}\langle R^2\rangle/(\langle l^2\rangle N)$

$$C_\infty = \frac{1 - \langle\cos\theta\rangle + (\langle\cos\theta\rangle^2 + \langle\sin\theta\rangle^2 - \langle\cos\theta\rangle)\langle\cos\phi\rangle}{1 - \langle\cos\phi\rangle(\langle\cos\theta\rangle^2 + \langle\sin\theta\rangle^2) + \langle\cos\theta\rangle(1 - \langle\cos\phi\rangle)} \quad (12)$$

and λ_1, λ_2, and λ_3 are the three eigenvalues of $\langle\mathbf{T}\rangle$

$$\lambda_{1/2} = -\frac{1}{2}\langle\cos\theta\rangle(1 - \langle\cos\phi\rangle) \pm \frac{1}{2}\{\langle\cos\theta\rangle^2(1 - \langle\cos\phi\rangle)^2 + 4\langle\cos\phi\rangle(\langle\cos\theta\rangle^2 + \langle\sin\theta\rangle^2)\}^{1/2}, \quad \lambda_3 = -\langle\cos\phi\rangle \quad (13)$$

These results (as well as the corresponding expression for $\langle R_g^2\rangle$) can be used for a check of the numerical procedures described above (see Figure 2) since $\langle\cos\theta\rangle$, $\langle\sin\theta\rangle$, and $\langle\cos\phi\rangle$ are straightforwardly obtained by carrying out the corresponding averages with $\exp[-\mathcal{H}_\theta(\theta_i)/k_BT]$ or $\exp[-\mathcal{H}_\phi(\phi_i)/k_BT]$, eqs 3 and 4, respectively.

Now, the inclusion of the LJ interaction, eq 5, can simply be carried out by calculating first the total energy $\mathcal{H}_{LJ}$ for each chain configuration which has been generated by the above procedure and then the appropriate Boltzmann weight with it, $\exp[-\mathcal{H}_{LJ}/k_BT]$, which is needed for the desired averaging. Note that the other contributions to the energy in eqs 1–4 do not enter the Boltzmann weight here, since they have already been taken into account in

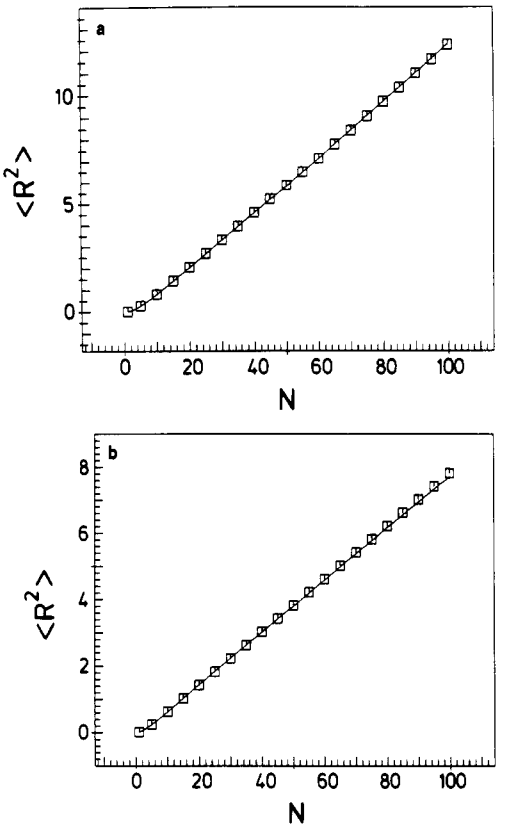

Figure 2. Mean-square end-to-end distance plotted vs N at (a) $T = 300$ K and (b) $T = 750$ K. The curves are the result of the Monte Carlo simulation, while the squares represent eq 11. All lengths are measured in nanometers.

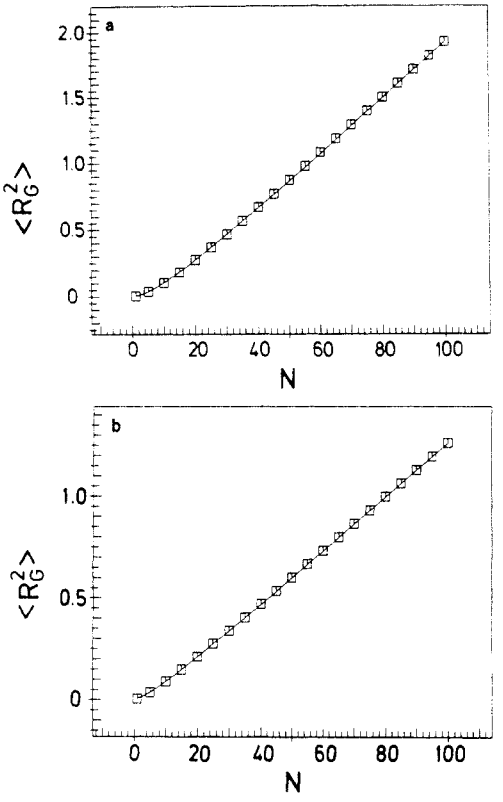

Figure 3. Mean-square gyration radius plotted vs N at (a) T = 300 K and (b) T = 750 K. The curves are the result of the Monte Carlo simulation, while the squares represent the results of a Flory-like theory.

the a priori probability $P(\{l_i,\theta_i,\phi_i\})$ with which the configurations $\{l_i, \theta_i, \phi_i\}$ have been generated, eq 6. Of course, $\mathcal{H}_{LJ}$ increases proportionally to the chain length N, and thus we have only considered $N \leq 50$ or $N \leq 60$ here. For such a choice of N the numerical effort necessary to obtain a small statistical error is still well manageable. If we wanted to study much longer chains, simple sampling techniques would be inefficient, as is well-known,[7,8] and other techniques to generate chain configurations such as, e.g., the pivot algorithm[32] might be used. Of course, in the absence of the LJ interaction the method based on eq 6 can generate configurations for arbitrarily long chains with the proper weight. Note also that we have typically generated on the order of 10^6 statistically independent chain configurations with this technique. A straightforward error analysis of our data shows that the relative error, i.e., $\langle (R^2 - \langle R^2 \rangle)^2 \rangle^{1/2} / \langle R^2 \rangle$, is typically on the order of 10^{-4} and that in almost all cases error bars would be smaller than the size of the symbols shown in the plots.

3. Numerical Results for the Model without Lennard-Jones Interaction

Figures 2 and 3 show typical data for the end-to-end distance and the gyration radius. The expected linear variation with the number of bonds N is clearly seen for $N \gtrsim 20$ (T = 300 K). For very small N the variation of these mean-square radii with N is nearly quadratic, reflecting the local stiffness of the chain. This is clearly seen when we calculate the persistence length[23] $a(T)$

$$a(T) \equiv \langle l \rangle \sum_{k=0}^{\infty} \langle \vec{e}_i \cdot \vec{e}_{i+k} \rangle = \frac{\langle l \rangle}{2}(1 + C_\infty) \qquad (14)$$

where $\vec{e}_i$ is a unit vector in the direction of the bond between monomers $i-1$ and i. The result is $a(T$=300 K) = 0.498 nm and $a(T$=750 K) = 0.338 nm, while at low temperatures $a(T)$ would be much larger [e.g., at T = 50 K we would have $a(T)$ = 24.877 nm, i.e., the persistence length would comprise about 200 monomers, noting that in the all-trans configuration each bond contributes 0.124 nm to the persistence length]. This local stiffness of the chain is also evident from the strongly nonmonotonic variation of $\langle R^2 \rangle / \langle R_g^2 \rangle$ with $1/N$ (Figure 4). While this ratio must reach 6 for $N \to \infty$, for intermediate N much larger value are obtained, particularly at low temperatures. This happens because for oligomers where the end-to-end distance and the persistence length are comparable $\langle R^2 \rangle$ increases much stronger with N than $\langle R_g^2 \rangle$ does.

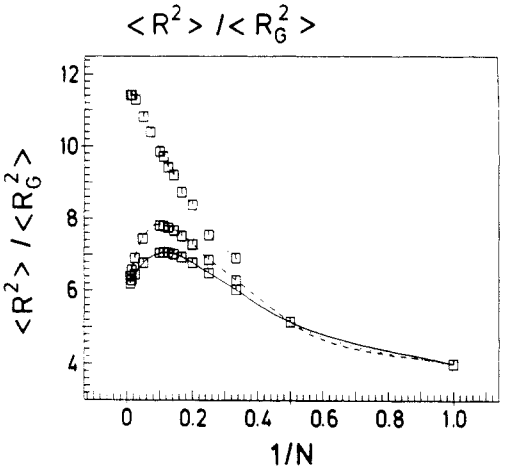

Figure 4. Ratio $\langle R^2 \rangle / \langle R_g^2 \rangle$ plotted vs $1/N$. The curves are the result of the simulation, and the squares represent the results of a Flory-like theory. Three temperatures are shown: T = 750 K (solid curve), T = 300 K (broken curve), and T = 50 K (dotted curve).

We have also obtained the static structure of the chains defined from

$$S(q,N) = \frac{1}{N+1}[\langle |\sum_{i=0}^{N} \exp(i\vec{q}\cdot\vec{r}_i)|^2 \rangle]_{|\vec{q}|} = 1 + \frac{2}{N+1}\sum_{i=0}^{N-1}\sum_{j=i+1}^{N} \frac{\langle \sin qr_{ij} \rangle}{qr_{ij}} \qquad (15)$$

where $[...]_{|q|}$ denotes a spherical average over the direction of $\vec{q}$ and compared the result to the Debye approximation[23]

$$S(q,N) = (N+1) f_D(q^2 \langle R_g^2 \rangle), \quad f_D(x) = \frac{2}{x}(x - 1 + \exp(-x)) \qquad (16)$$

See Figure 5. It is seen that eq 16 describes the numerical data reasonably well, apart from the regime of large q [where $qa(T) \approx 1$].

4. Numerical Results for the Model with Lennard-Jones Interaction

Figure 6 shows the data for $\langle R^2 \rangle$ and $\langle R_g^2 \rangle$ at T = 373 K with various choices for the range of the potential. It is seen that the radii are distinctly larger when the Lennard-Jones interaction is included than in the case where it is cut off completely (Δ_{max} = 3). For all choices of Δ_{max} the expected Gaussian law for large N, $\langle R^2 \rangle \sim \langle R_g^2 \rangle \sim N$, can be clearly recognized, however. At first sight it is surprising that the radii are largest when the LJ interaction is restricted to fourth-nearest neighbors along the chain. The interpretation for this finding is that the $g^{\pm}/g^{\mp}$ sequence is suppressed due to the repulsive part of the LJ interaction ("pentane effect"). However, including LJ interactions of somewhat longer range along the chain, many more configurations become possible where the attractive part

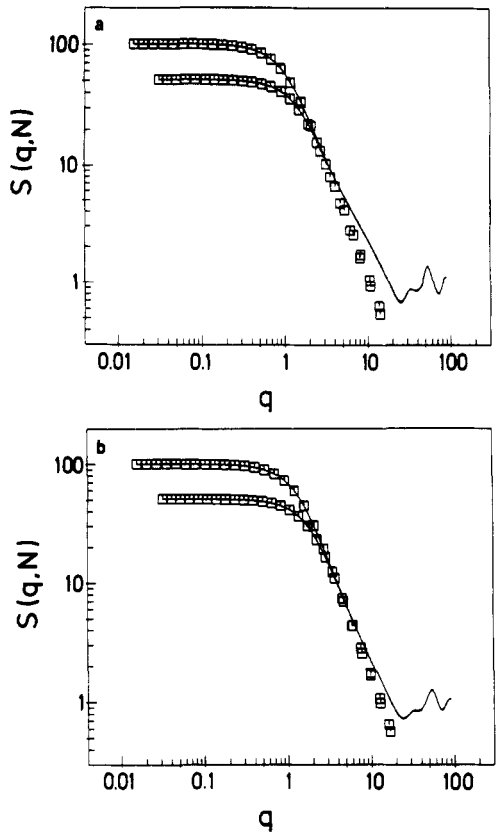

Figure 5. Structure factor $S(q,N)$ plotted vs wavenumber q for (a) $T = 300$ and (b) $T = 750$ K. The upper curve refers to $N = 100$ and the lower one to $N = 50$. The squares represent the Debye function, eq 16, using the gyration radius obtained from the Flory-like calculation.

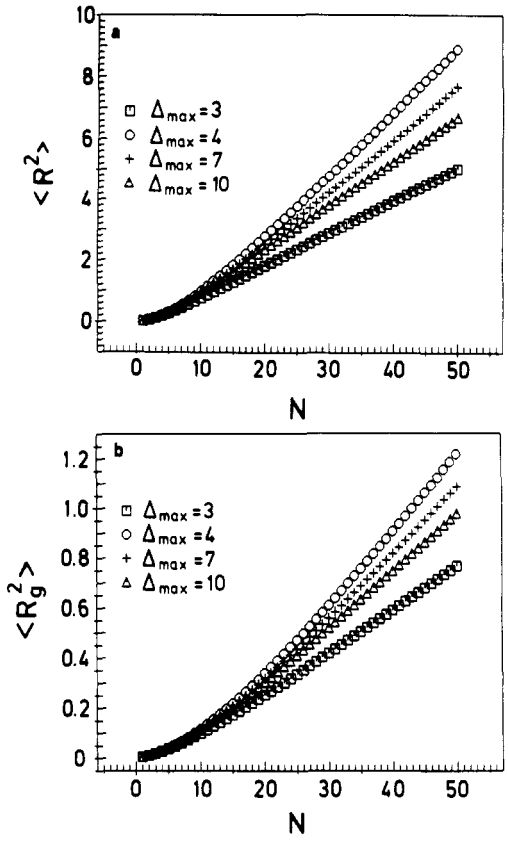

Figure 6. (a) Mean-square end-to-end distance $\langle R^2\rangle$ and (b) radius of gyration $\langle R_g^2\rangle$ plotted vs N at $T = 373$ K and various choices of the parameter Δ_{max} characterizing the range of the LJ interaction along the chain: $\Delta_{max} = 3$ (squares), $\Delta_{max} = 4$ (circles), $\Delta_{max} = 7$ (crosses), and $\Delta_{max} = 10$ (triangles).

of the LJ interaction starts to become felt. In fact, we have also carried out some runs where the LJ interaction was included between all segments further apart than three units along the chain and found that then the chain configurations tend to collapsed states for large N. This tendency toward collapse is responsible for the steady decrease of the radii with the increasing range of the LJ interaction. Figure 7 shows that the behavior at other temperatures is similar. In this context it is also an interesting question to what extent the characteristic ratio C_∞ is affected by the size of the cutoff of the LJ interaction. Therefore, we tried to estimate C_∞ from our simulation data for $N \leq 50$. We made a plot of C_N, defined by $C_N \equiv \langle R^2\rangle/N\langle l^2\rangle$, vs $1/N$ and assessed C_∞ by a linear extrapolation to $1/N = 0$ from the data points between $N = 20$ and $N = 50$ (Figure 8a). The choice to truncate the expansion of C_N after the first order

$$C_N = C_\infty + b/N + O(1/N^2) \qquad (17)$$

in order to approximate the real course in this range of chain lengths was motivated by a glance at a similar plot for the rotational isomeric state (RIS) model published in ref 23 and by the observation that the inclusion of a quadratic or cubic term in the upper trial function did not influence the result for C_∞ very much. Since C_N monotonically increases as $1/N \to 0$ toward C_∞,[23] one can expect that the estimated value for C_∞ represents a lower bound for the actual value which can only be determined reliably by a linear extrapolation if one generates chains with $N \gg 100$.[34,35] In Figure 8b the temperature dependence of the extrapolated C_∞ values for $\Delta_{max} = 4$ and $\Delta_{max} = 7$ is compared with that of the analytically available results for $\Delta_{max} = 3$ and for the RIS model (taken from ref 22). At first sight it might be surprising that the C_∞ values for

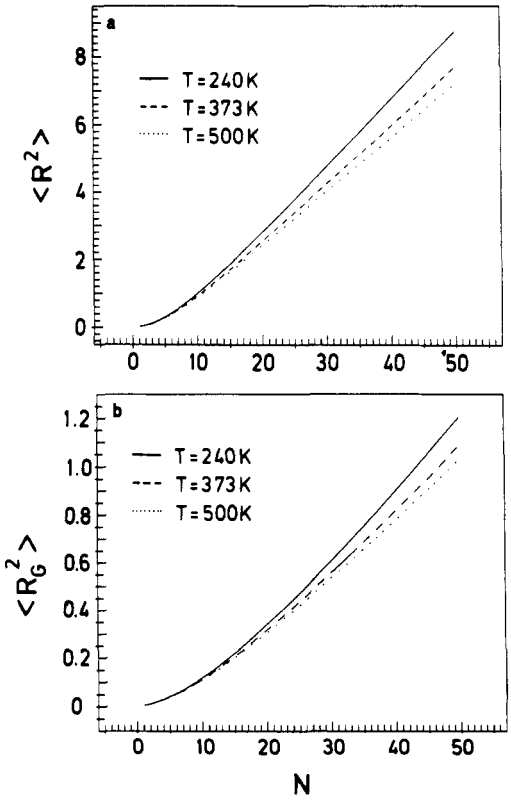

Figure 7. (a) Mean-square end-to-end distance $\langle R^2\rangle$ and (b) radius of gyration $\langle R_g^2\rangle$ plotted vs N at $T = 240$ K (solid curves), $T = 373$ K (broken curves), and $T = 500$ K (dotted curves) for $\Delta_{max} = 7$.

$\Delta_{max} = 4$ lie well above the RIS values, although both models take into account the same range of interaction

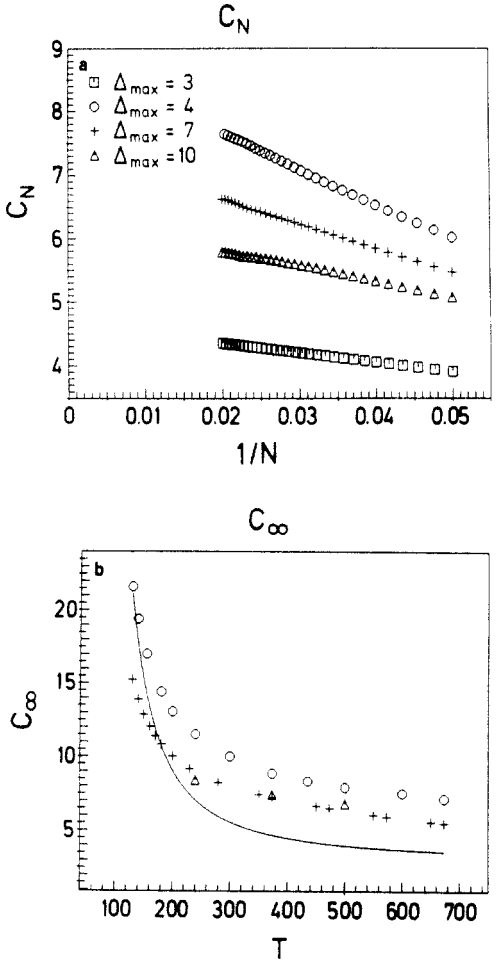

Figure 8. (a) Characteristic ratio $C_N \equiv \langle R^2 \rangle / (N\langle l^2 \rangle)$ plotted vs $1/N$ for $T = 373$ K and the same choices of the parameter Δ_{max} characterizing the range of the LJ interaction as in Figure 6. (b) Temperature dependence of C_∞. The solid curve represents eq 12 (where the LJ interaction is omitted). The circles represent data with $\Delta_{max} = 4$, and the triangles represent data with $\Delta_{max} = 7$. For comparison, results based on a simple rotational isomeric state (RIS) model for PE taken from ref 22 are included (crosses).

along the chain. However, this result becomes understandable if one realizes that the energy difference between the trans and the gauche states of the model from refs 15 and 16 is larger than that of the RIS model by a factor of 1.4. This is also the factor by which the C_∞ values or $\Delta_{max} = 4$ differ from those of the RIS model. Therefore, the difference in the dihedral potential is responsible for the stronger stretching of the chains in this model. This stiffness can only be reduced if one increases the cutoff of the LJ interaction to a Δ_{max} value of, say, 7 (Figure 8b). Then the results seem to be comparable to those of the RIS model and to the measured C_∞ values compiled in Table II, if one does not take into account the values for *p*-xylene and bis(2-ethylhexyl adipate). The high value $C_\infty = 10.3$ was obtained by light scattering, and the authors[36] remark that their light scattering data are generally too large, whereas the values $C_\infty = 5.2$ and $C_\infty = 5.3$ resulted from a viscosity measurement.[33] These two values seem to us to be too small, because all other C_∞ values were also obtained by viscosity measuements and they agree much better with each other.

5. Distribution Functions $P_n(l)$ and $P_n(\vartheta)$

Recently it has been proposed to use groups of n successive monomers as subunits to characterize the structure of polymer chains on supramolecular scales intermediate between the monomer size and the coil size.[22]

Table II
Survey of the Characteristic Ratios C_∞ and the Θ-Temperatures for Several Solvents (Taken from Reference 33)

solvent	Θ-temp, °C	C_∞
p-xylene	~100	5.3
decalin	140	6.8
bis(2-ethylhexyl adipate)	145	5.2
	145	10.3
biphenyl	127.5	7.0
dodecanol	137.3	6.8
	138	6.9
diphenylmethane	142.2	6.9
decanol	153.3	7.6
diphenyl ether	161.4	6.4
octanol	180.1	6.4
biphenyl	127.5	7.1
diphenylmethane	142.2	7.0

The distribution function $P_n(l)$ for the distance l between the centers of gravity of such units formed from n monomers each, as well as the distribution $P_n(\vartheta)$ of the angle between two successive effective bonds defined in this way, is useful because it provides a means for a mapping of a chemically realistic model on a lattice model[20] and also yields a new way to characterize more precisely the local structure of chains on such intermediate length scales. Thus we also present some information on these distribution functions here.

Figure 9 presents $P_n(l)$ (l is measured in units of l_0) for $n = 5$ and $n = 10$, while Figure 10 presents $P_n(\vartheta)$ for $n = 5$ and $n = 10$. From Figures 9a,b and 10a it is seen that for the choice when the LJ interactions is completely cut off there is considerable weight in the distribution for small bond lengths and bond angles, which is suppressed if the LJ interaction is included for short distances (choices of Δ_{max} from $\Delta_{max} = 4$ to $\Delta_{max} = 7$), which tends to make the chain stiffer on short scales. Adding LJ interactions of still longer range adds weight to the distribution on short lengths l and small angles ϑ, again reflecting the increasing tendency toward collapse. These results strengthen our interpretation given on the behavior of $\langle R^2 \rangle$ and $\langle R_g^2 \rangle$ with the increasing range of the LJ interaction. Parts c and b of Figure 9 and the respective parts of Figure 10 show the temperature variation of the coarse-grained distance and angle distribution functions when the cutoff of the LJ potential is held fixed at $\Delta_{max} = 7$. As is expected from the discussion of Figures 9a,b and 10a,b the LJ potential keeps the chain stiff on short length scales and thus does not allow a large temperature variation of the distance distribution function $P_5(l)$. However, if one increases the number of monomers contributing to one center of gravity, one also increases the flexibility of the coarse-grained chain and therefore the response to a temperature change (i.e., contraction of the chain) should be larger. This is exemplified by the distance distribution function $P_{10}(l)$. Note that this statement is not in contradiction to Figure 10c,d, where the angle distribution function apparently remains nearly invariant, when the temperature is increased, since the coarse-grained "bond angle" is determined by twice as much chemical monomers than the corresponding "bond length" of the coarse-grained chain. Therefore, correlations are averaged out more efficiently, and the angle distribution function reaches its limiting behavior more quickly.[22]

6. Concluding Remarks

In this paper we have shown that the configurational statistics of short isolated chains (such as PE with $N \leq 50$ monomers) can be studied very conveniently with a

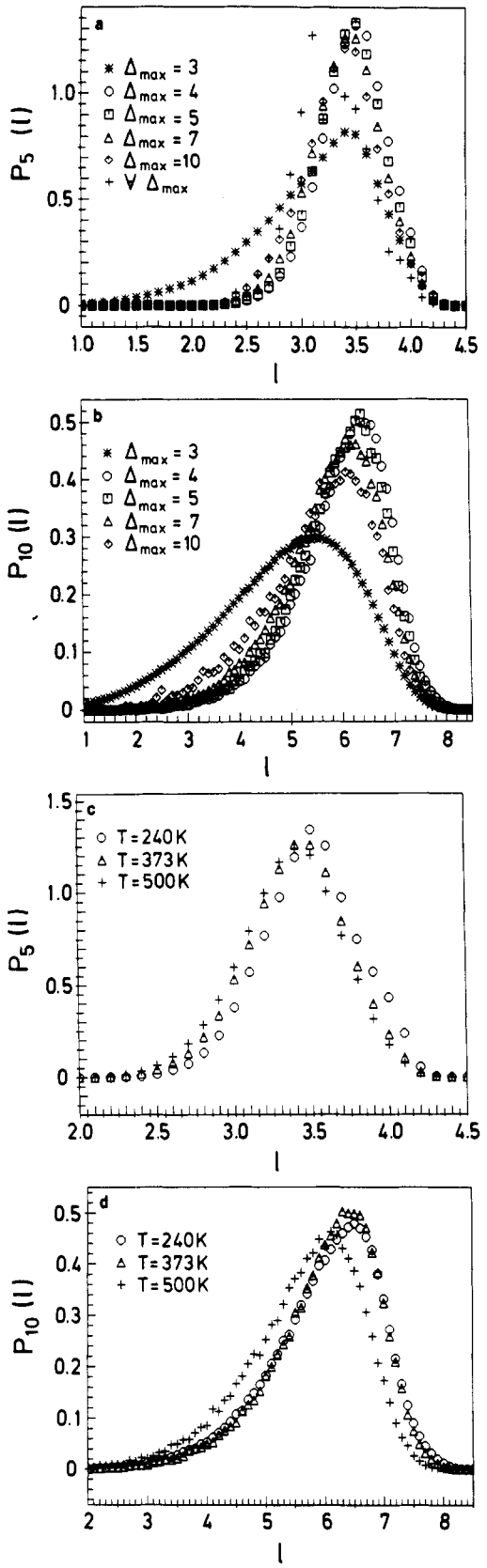

Figure 9. (a) Distribution function $P_5(l)$ vs l (measured in units of l_0) for T = 373 K and various choices for the range of the LJ interaction: no LJ interaction (asterisks); Δ_{max} = 4 (circles); Δ_{max} = 5 (squares); Δ_{max} = 7 (triangles); Δ_{max} = 10 (diamonds); unrestricted LJ interactions (crosses). (b) Same as a but for n = 10 and without unrestricted LJ interaction. (c) $P_5(l)$ vs l for Δ_{max} = 7 and the three temperatures T = 240 K (circles), T = 373 K (triangles), and T = 500 K (crosses). (d) Same as c but for $P_{10}(l)$.

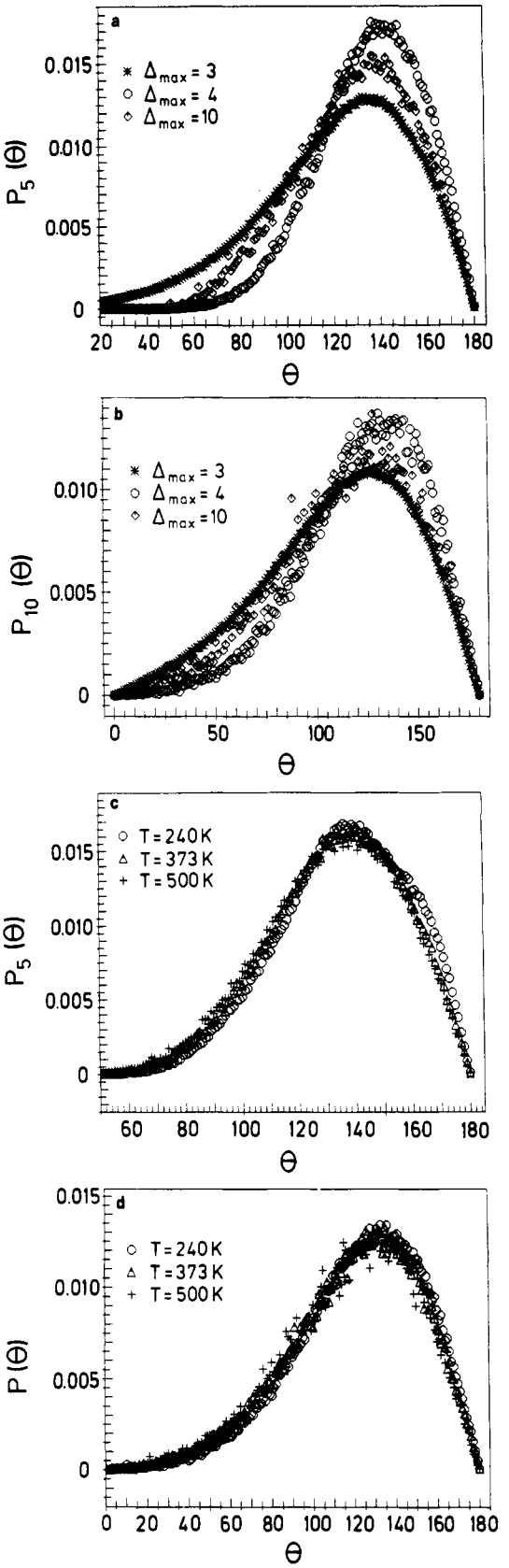

Figure 10. (a) Distribution function $P_5(\vartheta)$ vs ϑ for T = 373 K and various choices for the range of the potential: no LJ interaction (asterisks); Δ_{max} = 4 (circles); Δ_{max} = 10 (diamonds). Results for intermediate choices of Δ_{max} are omitted for the sake of clarity in this figure. (b) Same as a but for $P_{10}(\vartheta)$. (c) $P_5(\vartheta)$ vs ϑ for Δ_{max} = 7 and the three temperatures T = 240 K (circles), T = 373 K (triangles), and T = 500 K (crosses). (d) Same as c but for $P_{10}(\vartheta)$.

generalized simple sampling Monte Carlo method. In this technique, the separable parts of the potential (i.e., the potentials for bond length variations, bond angle variations, and the torsional potential) are taken into account in the construction step for the chain configurations, and

only the nonseparable part of the potential describing van der Waals or Coulomb forces between nonbonded atoms is sampled by the appropriate Boltzmann factor. We have checked the accuracy of our procedure in the simple case where the nonbonded LJ interaction was completely turned off, and the end-to-end distance was calculated exactly, and shown to be in excellent agreement with the Monte Carlo data. In the case where the LJ interaction was included, no exact results are available for comparison, but due to the simple sampling technique the different configurations generated are statistically uncorrelated, and hence the accuracy of the results could be assessed by standard statistical analysis.

Although the presented simple sampling is straightforward enough to be possibly generalized to other polymers which are chemically more complex than PE, it is clear from our study that one must be very cautious in associating any inference from such a study of a single isolated chain in "vacuum" to the properties of chains in Θ-solvent or a melt; however, our data do show that the results depend very sensitively on the extent to which the nonbonded interactions (modeled by LJ interactions here) are included. If they are cut off completely, local backfolds (configurations of the $g^{\pm}/g^{\mp}$ type) get too much weight, which certainly do not occur in either Θ-solvent or a melt; if one cuts off the interaction after the fourth-nearest neighbor, a large degree of local chain stiffnes is introduced, which probably is also chemically unrealistic. If a much larger range of the LJ interaction is admitted, a crossover toward collapsed chain configurations starts to set in. We do not see any reason that any of these choices faithfully represents the chain configuratinos in a Θ-solution or a melt, where the solvent (or the other chains) gradually screens out the LJ interaction. Rather than the sharp cutoff of the LJ interaction used in the present work, one might also damp it out more smoothly with a factor $\exp(-|i - j|\Delta_{max})$, say. In view of the uncertainties that still exist[22] on the optimal choice of potentials for PE, it is not clear at present whether this would give better results. Thus we feel that the real value of the methods presented here is not so much to directly make predictions for bulk polymeric materials but rather to provide methods which can be used as input information for more complete simulations of multichain systems[20] and to provide standards against which other simulation methods can be checked.

Acknowledgment. K.Q. thanks the Deutsche Forschungsgemeinschaft (DFG) and the Council for Education of the People's Republic of China, Beijing, China, for providing him with a research fellowship. This research was also funded in part by the Deutsche Forschungsgemeinschaft and by the Bundesministerium für Forschung und Technologie (BMFT) under Grant No. 03M4028 and the BAYER AG.

References and Notes

(1) Ciccotti, G., Hoover, W. G., Eds. *Molecular Dynamics Simulations of Statistical Mechanical Systems*; North-Holland, Amsterdam, The Netherlands, 1986.
(2) Hockney, R. W.; Eastwood, J. W. *Computer Simulation Using Particles*; Hilger: Bristol, U.K., 1988.
(3) Ciccotti, G., Frenzel, D., McDonald, I. R. Eds. *Simulation of Liquids and Solids*; North-Holland: Amsterdam, The Netherlands, 1987.
(4) Kremer, K.; Grest, G. S. *J. Chem. Phys.* **1990**, *92*, 5057 and references therein.
(5) Binder, K., Ed. *Monte Carlo Methods in Statistical Physics*; Springer: Berlin, 1979.
(6) Binder, K., Ed. *Applications of the Monte Carlo Method in Statistical Physics*; Springer: Berlin, 1984.
(7) Binder, K.; Heermann, D. W. *Monte Carlo Simulation in Statistical Physics: An Introduction*; Springer: Berlin, 1988.
(8) Kremer, K.; Binder, K. *Comput. Phys. Rep.* **1988**, *7*, 259.
(9) Baumgärtner, A. *Annu. Rev. Phys. Chem.* **1984**, *35*, 419. Baumgärtner, A. Reference 6, Chapter 5.
(10) Binder, K. In *Molecular Level Calculations of the Structure and Properties of Non-Crystalline Polymers*; Bicerano, J., Ed.; Marcel Dekker: New York, in press.
(11) Ryckaert, J. P.; Bellemans, A. *Chem. Phys. Lett.* **1975**, *30*, 123; *Faraday Discuss.* **1978**, *66*, 95.
(12) Helfand, E.; Wasserman, Z.; Weber, T. *Macromolecules* **1980**, *13*, 526.
(13) Clarke, J. H. R.; Brown, D. *Mol. Phys.* **1986**, *58*, 815.
(14) Clarke, J. H. R.; Brown, D. *Mol. Simul.* **1989**, *3*, 27.
(15) Rigby, D. J.; Roe, R. J. *J. Chem. Phys.* **1987**, *87*, 7285.
(16) Rigby, D. J.; Roe, R. J. *J. Chem. Phys.* **1988**, *88*, 5280; *Macromolecules* **1989**, *22*, 2259.
(17) Taluchi, Roe, R. J. *J. Chem. Phys.* **1991**, *94*, 7446 and 7458.
(18) Jung, B.; Schürmann, B. L. *Macromolecules* **1989**, *22*, 477; *Macromol. Chem., Rapid Commun.* **1989**, *10*, 419.
(19) Theodorou, D. N.; Suter, U. W. *Macromolecules* **1985**, *18*, 1467; **1986**, *19*, 379.
(20) Paul, W.; Binder, K.; Kremer, K.; Heermann, D. W. preprint.
(21) Binder, K. Proceedings of the Europhysics Conference on Computational Physics, Amsterdam, The Netherlands, 1990; *Int. J. Mod. Phys. C* **1991**, *2*, 263.
(22) Baschnagel, J.; Binder, K.; Paul, W.; Laso, M.; Suter, U. W.; Batoulis, I.; Jilge, W.; Bürger, T. *J. Chem. Phys.*, in press.
(23) Flory, P. J. *Statistical Mechanics of Chain Molecules*; Interscience: New York, 1969.
(24) Doi, M.; Edwards, S. F. *The Theory of Polymer Dynamics*; Clarendon Press: Oxford, U.K., 1986.
(25) Metropolis, N.; Rosenbluth, A. W.; Rosenbluth, M. N.; Teller, A. H.; Teller, E. *J. Chem. Phys.* **1953**, *21*, 1087.
(26) de Gennes, P.-G. *Scaling Concepts in Polymer Physics*; Cornell University Press: Ithaca, NY, 1979.
(27) Ryckaert, J. P.; McDonald, I. R.; Klein, M. L. In *Computer Simulation of Polymers*; Roe, R. J., Ed.; Prentice-Hall: Englewood Cliffs, NJ, 1991; p 70. Doherty, D. C.; Hopfinger, A. J. In *Computer Simulation of Polymers*; Roe, R. J., Ed.; Prentice-Hall: Englewood Cliffs, NJ, 1991; p 55.
(28) For more details, see: Baschnagel, J. Diplomarbeit, Universität Mainz, 1990, unpublished.
(29) Abe, A.; Jemigan, R. L.; Flory, P. J. *J. Am. Chem. Soc.* **1966**, *88*, 631.
(30) Milchev, A.; Heermann, D. W.; Binder, K. *J. Stat. Phys.* **1986**, *44*, 749.
(31) Almarza, N. G.; Enrico, E.; Alonso, J.; Bermejo, F. J. *Mol. Phys.* **1990**, *70*, 485.
(32) Madras, N.; Sokal, A. *J. Stat. Phys.* **1988**, *50*, 109.
(33) Brandrup, J., Immergut, E. H., Ed. *Polymer Handbook*; Wiley: New York, 1975.
(34) Mattice, W. L.; Carpenter, D. K. *Macromolecules* **1976**, *9*, 53.
(35) Suter, U. W.; Flory, P. J. *Macromolecules* **1975**, *8*, 765.
(36) Kotera, A.; Matsuda, H.; Wada, A. *Rep. Prog. Polym. Phys. Jpn.* **1965**, *8*, 5.

Registry No. $(CH_2{=}CH_2)_x$ (homopolymer), 9002-88-4.